EURASIAN JOURNAL OF MEDICAL AND NATURAL SCIENCES
Innovative Academy Research Support Center
IF = 7.921 www.in-academy.uz

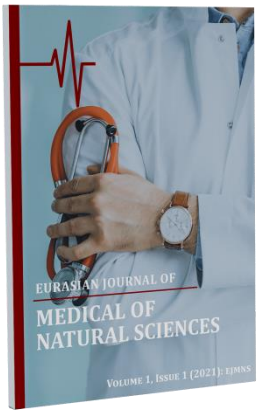

RAMAN SPECTROSCOPY AND IMAGING IN CANCER DIAGNOSTICS

Malikov Murod Rasulovich
Senior lecturer at the Alfraganus University
Email address: malikovmurod55@mail.ru
Orcid ID: 0009-0008-1406-8977
https://doi.org/10.5281/zenodo.14729221

ARTICLE INFO

Received: 18th January 2025
Accepted: 23rd January 2025
Online: 24th January 2025

KEYWORDS

Raman Spectroscopy, Coherent Raman Scattering (CRS), Stimulated Raman Scattering (SRS), Surface-Enhanced Raman Scattering (SERS), Cancer Diagnosis, Multimodal Imaging, Hyperspectral Imaging, Biomolecular Analysis, Tumor Margins.

ABSTRACT

Raman scattering has long been utilized to analyze chemical compositions in biological systems. With its high chemical specificity and noninvasive detection capabilities, Raman scattering has seen significant use in cancer screening, diagnosis, and intraoperative surgical guidance over the past decade. To address the limitations of weak signals in spontaneous Raman scattering, advancements such as coherent Raman scattering and surface-enhanced Raman scattering have been developed and applied in cancer research. This review highlights innovative applications of Raman scattering in cancer diagnosis and explores their potential for clinical adoption.

1.Introduction

Cancer remains a major global health challenge, creating an urgent need for advanced techniques in screening, diagnosis, and surgical guidance. Raman scattering, which examines chemical compositions in cells and tissues by interacting with molecular vibrational modes, provides a noninvasive and label-free method for detecting disease-related changes in molecular structures. These attributes make Raman spectroscopy an attractive tool for cancer diagnostics. However, the inherently weak signal of spontaneous Raman scattering ($\sim 10-30\ cm^2$ per molecule) necessitates long integration times, which limits its utility in biological and medical applications (as illustrated in Figure 1(a)).

EURASIAN JOURNAL OF MEDICAL AND NATURAL SCIENCES
Innovative Academy Research Support Center
IF = 7.921 www.in-academy.uz

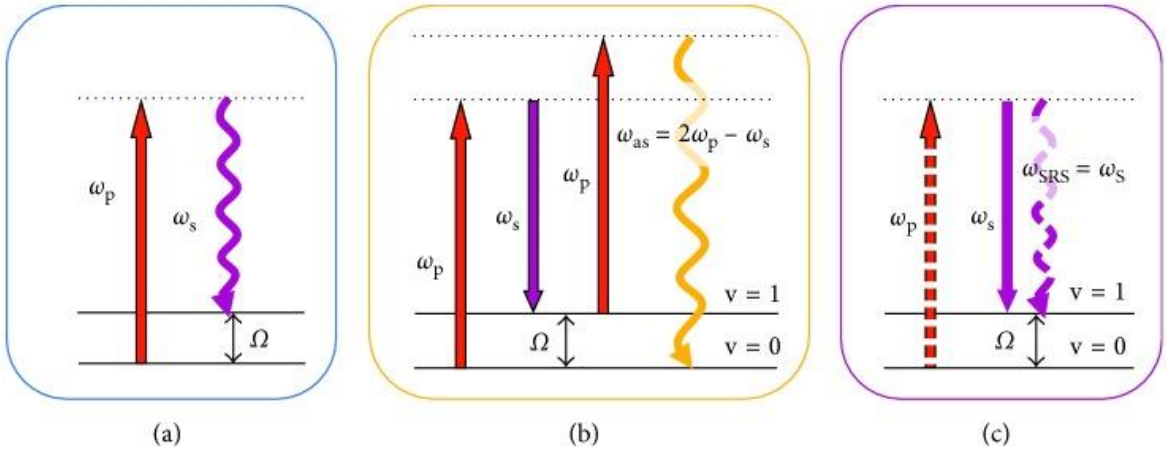

Figure 1. Energy Diagrams for Spontaneous Raman Scattering (a), Coherent Anti-Stokes Raman Scattering (CARS) (b), and Stimulated Raman Scattering (SRS) (c).

To enhance the signal intensity of Raman scattering, coherent Raman scattering (CRS) microscopy was developed. As illustrated in Figures 1(b) and 1(c), most CRS imaging experiments utilize two excitation fields, referred to as the pump (ωp) and Stokes (ωs) frequencies. When the frequency difference (ωp − ωs) aligns with a molecular vibrational mode, coherent anti-Stokes Raman scattering (CARS) occurs at the frequency "(ωp − ωs) + ωp," and stimulated Raman scattering (SRS) occurs at the frequencies "ωs" or "ωp" simultaneously. CRS microscopy enables imaging speeds approximately 1,000 times faster than line-scan Raman microscopy and 10,000 times faster than point-scan Raman microscopy due to its significantly higher signal levels.

The key advantage of SRS over CARS lies in the absence of a nonresonant background, making SRS microscopy a highly sensitive and quantitative tool for biochemical imaging. Additionally, SRS can operate under ambient light conditions. Meanwhile, advancements in nanotechnology have also led to the development of surface-enhanced Raman scattering (SERS), which significantly amplifies Raman signals, albeit in a labeling-based manner.

With these enhanced capabilities, Raman scattering-based techniques have a wide range of applications in cancer diagnosis. This review explores recent advancements and applications of Raman scattering techniques in cancer research, focusing on three key methods—spontaneous Raman spectroscopy, CRS, and SERS—and their potential to bridge the gap between laboratory research and clinical practice.

2. Spontaneous Raman Scattering for Cancer Diagnosis

2.1. Ex Vivo

2.1.1. Biofluids

Bhattacharjee et al. utilized Raman spectroscopy to diagnose breast cancer using urine samples from a rat model, achieving classification efficiencies of 80% and 72% through principal component analysis (PCA) and principal component-linear discriminant analysis (PC-LDA), respectively. Similarly, Elumalai et al. employed Raman spectroscopy to distinguish between normal and oral cancer patients using urine samples, demonstrating an accuracy of 93.7%, a sensitivity of 98.6%, and a specificity of 87.1% with PCA-based linear discriminant

analysis. Additionally, Sahu et al. analyzed serum samples from oral cancer patients and healthy subjects, identifying Raman bands related to beta-carotene and DNA content as potential diagnostic markers for oral cancer.

2.1.2. Tissues

(1) Gastrointestinal Cancer

Almond et al. evaluated endoscopic Raman spectroscopy for grading Barrett's esophagus-associated high-grade dysplasia and adenocarcinoma. Their study, conducted on 673 ex vivo esophageal tissue samples from 62 patients, demonstrated a sensitivity of 86% and a specificity of 88%. Hsu et al. differentiated gastrointestinal stromal tumors from gastric adenocarcinomas and normal mucosae using confocal Raman microspectroscopy, identifying distinct Raman signals related to phospholipids and protein structures. They further classified four histological types of gastric adenocarcinomas—papillary, tubular, mucinous, and signet ring cell adenocarcinomas—using this method. Petersen et al. used Raman fiber-optic measurements on colon biopsy samples obtained during colonoscopies, achieving a diagnostic accuracy of over 70%.

(2) Skin Cancer

Nijssen et al. demonstrated that Raman spectroscopy could differentiate basal cell carcinoma from surrounding tissue in unstained frozen sections of 15 specimens. Gniadecka et al. explored its application for melanoma diagnosis, using neural network analysis to identify structural changes in proteins and lipids. Their study achieved 85% sensitivity and 99% specificity. Bodanese et al. applied Raman spectroscopy to identify malignant basal cell carcinoma and melanoma in vitro, with proteins, lipids, and melanin accounting for 95.4% of spectral variation. They also found that PCA-based models outperformed biochemical models in sensitivity and specificity. Furthermore, Nijssen et al. validated the use of the high-wavenumber region in Raman spectroscopy for accurate basal cell carcinoma diagnosis, circumventing the complexity of fiber-optic probes in the fingerprint region.

(3) Breast Cancer

Frank et al. were among the first to apply Raman spectroscopy to breast cancer diagnosis, identifying spectral differences in lipids and carotenoids between normal and cancerous biopsies. Subsequent studies revealed weaker lipid bands and more prominent collagen bands in cancerous tissues. Haka et al. found that type II microcalcifications in malignant ducts contained less calcium carbonate and more protein than those in benign ducts. Later, using Raman spectroscopy on samples from 58 patients, they developed a linear combination model incorporating nine representative spectra of breast tissue's morphological and chemical features. This model achieved 94% sensitivity and 96% specificity, with fat and collagen serving as key diagnostic parameters.

(4) Lung Cancer

Huang et al. performed near-infrared (NIR) Raman spectroscopy on tissue specimens from patients and identified that the ratio of Raman intensities at 1,445 to 1,655 cm^{-1} could distinguish malignant bronchial tissue. Magee et al. designed a miniaturized fiber-optic Raman probe compatible with the working channel of a bronchoscope, enabling accurate classification of normal and malignant lung tissues in ex vivo studies.

(5) Brain Cancer

Koljenovic et al. demonstrated that Raman spectroscopy could differentiate vital tumor tissue from necrotic areas in unfixed cryosections of glioblastomas obtained from 20 patients. Later, the authors extended their research by using high-wavenumber Raman spectroscopy with a single fiber-optic probe setup to analyze brain tissue slices from seven pigs, showcasing its potential as a tool for intraoperative guidance. Krafft et al. applied a spectral unmixing algorithm to identify cell density and nuclei in Raman images of primary brain tumor tissue, revealing that the morphological and compositional data provided complementary insights to histopathology for improved diagnostics.

2.2. In Vivo

2.2.1. Animal Models

Kirsch et al. demonstrated the capability of Raman spectroscopy to detect intracerebral tumors in vivo by mapping the brain surface with an accuracy of approximately 250 μm. In parallel, Beljebbar et al. showed that Raman spectroscopy could differentiate normal brain tissues from tumors with 100% accuracy in a C6 glioblastoma animal model, primarily by detecting variations in lipid signals.

2.2.2. Studies in Humans

(1) Gastrointestinal Cancer

The Huang group has made significant strides in applying Raman spectroscopy for in vivo gastrointestinal cancer diagnosis during clinical endoscopic examinations. They developed a narrow-band image-guided Raman endoscopy technique for diagnosing gastric dysplasia, achieving a sensitivity of 94.4% and a specificity of 96.3%. Key diagnostic features included albumin, nucleic acids, phospholipids, and histones. Bergholt et al. combined novel fiber-optic Raman spectroscopy with semiquantitative spectral modeling, revealing progressive biochemical changes in gastric tissues during preneoplastic and neoplastic transformation. By analyzing 1,277 in vivo Raman spectra from 83 gastric patients, they achieved sensitivities of 83.33% for dysplasia and 84.91% for adenocarcinoma, with respective specificities of 95.80% and 95.57%. Additionally, they applied Raman spectroscopy to colorectal tissues, achieving a diagnostic accuracy of 88.8% using partial least squares-discriminant analysis. Shim et al. also demonstrated the feasibility of NIR Raman spectroscopy for use during clinical gastrointestinal endoscopy.

(2) Breast Cancer

Haka et al. applied in vivo Raman spectroscopy during partial mastectomy surgeries in nine patients for margin assessment. Using their established diagnostic algorithm, they achieved high sensitivity and specificity in differentiating normal and cancerous tissues. Brozek-Pluska et al. investigated noncancerous and cancerous breast tissues from the same patients and identified significant differences in carotenoids, proteins, and lipids, particularly unsaturated fatty acids, between the two tissue types.

(3) Brain Cancer

Desroches et al. characterized a handheld Raman spectroscopy system to enhance the precision of glioma surgery by maximizing resected cancer tissue volume. Initial measurements from normal, necrotic, and cancerous brain tissues collected from 10 patients showed an accuracy of 87% in distinguishing necrotic tissue from normal and cancerous tissue. In the same year, Jermyn et al. developed a handheld contact Raman spectroscopy

probe for live, localized detection of cancer cells in the human brain. Using this technique, they achieved a sensitivity of 93% and a specificity of 91% for identifying cancer cells.

(4) Cervical Cancer

The Huang group has conducted extensive research on detecting cervical precancer using in vivo Raman spectroscopy. They demonstrated that combining near-infrared (NIR) Raman spectroscopy with a genetic algorithm-partial least squares-discriminant analysis could identify seven diagnostically significant Raman bands associated with proteins, nucleic acids, and lipids, achieving an accuracy of 82.9% for precancer detection. Subsequently, they showed that NIR confocal Raman spectroscopy could enhance diagnostic performance with improved sensitivity and specificity. In a separate study involving 93 participants under clinical supervision, Shaikh et al. observed high collagen levels in normal cervical tissue and prominent DNA signals in tumors. Using principal component-linear discriminant analysis, they achieved 97% accuracy in distinguishing normal tissues from tumors.

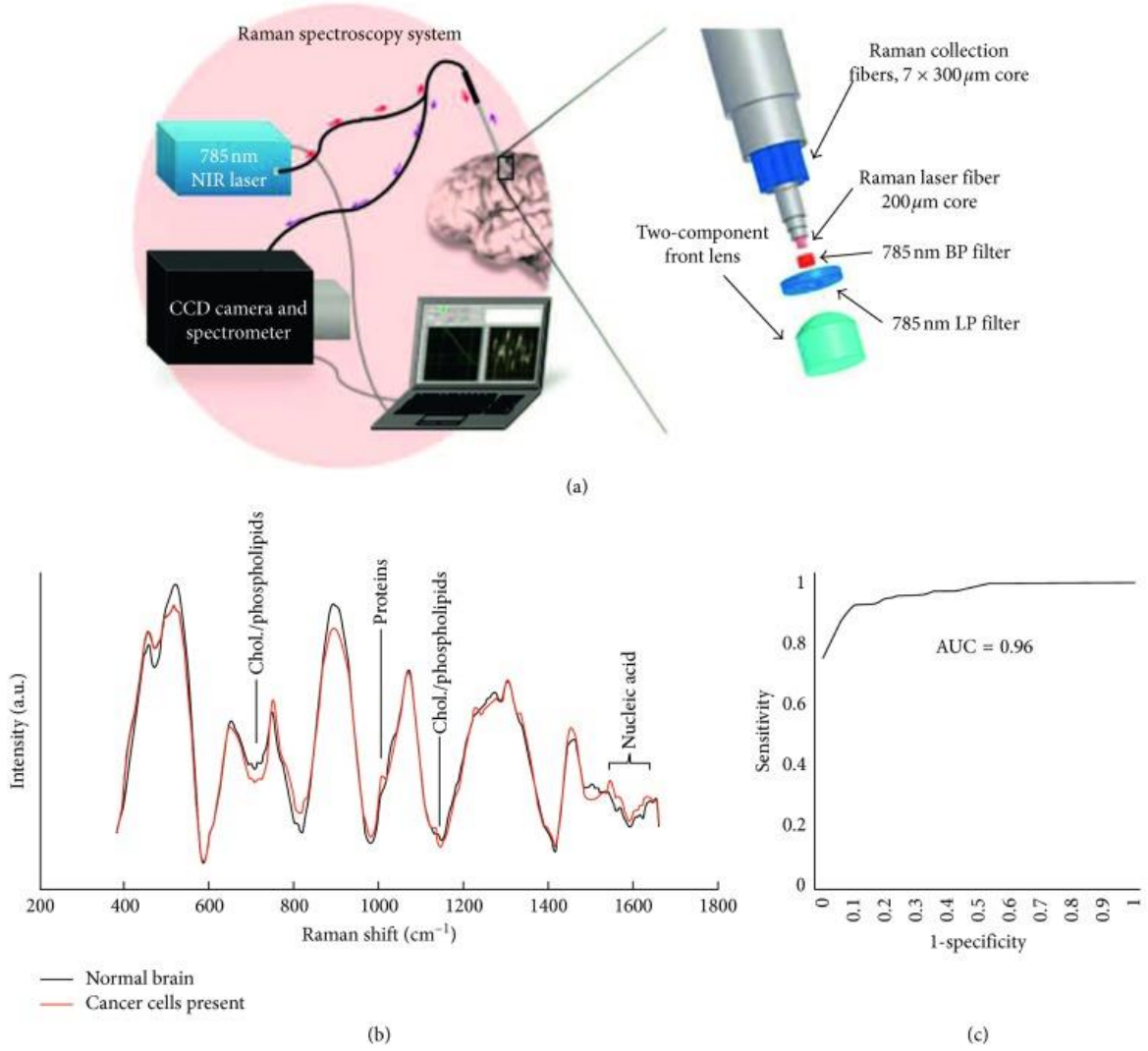

Figure 2. Handheld Contact Raman Spectroscopy Probe for Real-Time, Localized Detection of Cancer Cells in the Human Brain. (a) System Configuration; (b) Raman Spectra Differentiating Normal and Cancerous Brain Cells; (c) Diagnostic Sensitivity and Specificity.

(5) Skin Cancer

Lui et al. assessed a real-time Raman spectroscopy system for in vivo skin cancer diagnosis. The study involved 518 benign and malignant lesions from 453 patients, with each lesion measured in just one second. The system successfully differentiated benign, precancerous, nonmelanoma, and melanoma lesions, achieving sensitivities between 95% and 99% and specificities ranging from 15% to 54%.

3. Coherent Raman Scattering for Cancer Diagnosis

3.1. Ex Vivo

3.1.1. Brain Cancer

The Xie group has made significant advancements in developing coherent Raman scattering (CRS) microscopy for neuropathological diagnostics. Evans et al. demonstrated the capability of coherent anti-Stokes Raman scattering (CARS) microscopy to identify normal brain structures and primary gliomas in fresh, unfixed, and unstained brain tissues. Later, Freudiger et al. introduced multicolor coherent Raman imaging, which visualized lipid and protein signals from CH_2 and CH_3 vibrations in fresh brain tissue. The resulting multicolor images closely resembled corresponding histopathological images. Uckermann et al. utilized CARS imaging at the C-H molecular vibration region to analyze brain tissues from an orthotopic mouse model and human glioblastoma, successfully delineating tumor margins and infiltrations based on lipid content with cellular resolution. Recently, Ji et al. applied stimulated Raman scattering (SRS) microscopy to study tumor infiltration in fresh surgical specimens from 22 neurosurgical patients. The study revealed that SRS could detect tumor infiltration with high agreement to H&E staining. By quantitatively analyzing cellularity, axonal density, and the protein-to-lipid ratio, the authors developed a classifier achieving 97.5% sensitivity and 98.5% specificity for tumor infiltration detection.

3.1.2. Lung Cancer

The Wong group pioneered the use of CARS microscopy to differentiate lung cancer from nonneoplastic lung tissues. By analyzing 92 fresh frozen lung tissue samples with established pathological knowledge, they achieved a sensitivity of 91% and a specificity of 92%. Additionally, by integrating deep learning with CARS imaging, the group further advanced automated differential diagnosis of lung cancer.

3.2. In Vivo

3.2.1. Animal Models

Ji et al. recently demonstrated that SRS microscopy could accurately delineate glioma infiltration in animal models by identifying histoarchitectural and biochemical differences. Their findings showed excellent agreement between SRS microscopy and hematoxylin and eosin (H&E) staining for detecting glioma infiltration (kappa = 0.98). The group also applied SRS microscopy during live surgeries to precisely identify tumor margins. Subsequently, the Ji group developed dual-phase SRS microscopy for real-time two-color imaging, matching the speed of single-color SRS. This approach enabled accurate real-time histology in vivo in both transmission and epi-detection modes.

3.2.2. Studies in Humans

Orringer et al. introduced a fiber-laser-based SRS microscopy system capable of performing rapid intraoperative histology on unprocessed surgical specimens from 101 neurosurgical patients. Their findings showed exceptional concordance between SRS

microscopy and conventional histology for diagnosis prediction (κ > 0.89), achieving an accuracy exceeding 90%. Building on this, Hollon et al. applied the technique to the intraoperative diagnosis of pediatric brain tumors, demonstrating near-perfect diagnostic concordance (κ > 0.90) and an accuracy ranging from 92% to 96%.

4. Surface-Enhanced Raman Scattering (SERS) for Cancer Diagnosis

4.1. Ex Vivo

Dai et al. utilized SERS to distinguish human oral cancer cells from normal fibroblast cells in vitro by identifying the characteristic Raman signal of adenine at 735 cm^{-1}. Grubisha et al. developed a SERS-based immunoassay, enabling rapid femtomolar-level detection of prostate-specific antigen for prostate cancer screening. Li et al. applied SERS combined with support vector machine analysis to study serum samples from 93 prostate cancer patients and 68 healthy volunteers, achieving a diagnostic accuracy of 98.1%. Del Mistro et al. conducted a preliminary investigation into prostate cancer detection using SERS analysis of urine samples, achieving 100% sensitivity, 89% specificity, and an overall diagnostic accuracy of 95% through principal component and linear discriminant analysis.

Feng et al. analyzed purified whole proteins from human saliva using SERS spectroscopy, achieving 90.2% accuracy in detecting nasopharyngeal cancer. Additionally, they demonstrated that SERS could differentiate between healthy individuals, benign breast tumor patients, and malignant breast tumor patients, with sensitivities exceeding 70% and specificities over 80%.

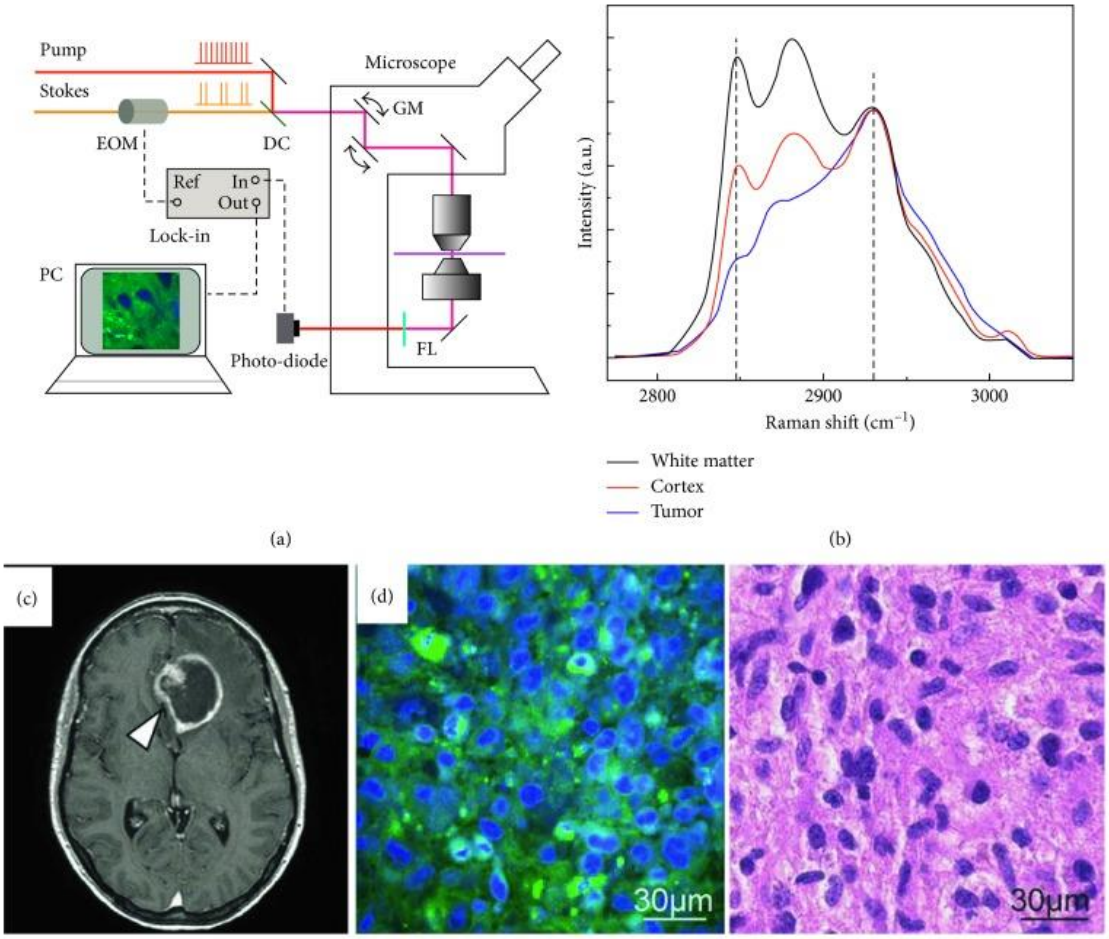

Figure 3. SRS microscopy illustrating glioma infiltration in animal models: (a) System setup; (b) Raman spectra of white matter, cortex, and tumor; (c) MRI image of a mouse brain; (d) SRS image paired with the corresponding H&E-stained image of glioma tissue. Adapted with permission.

4.2. In Vivo

4.2.1. Animal Models

Mohs et al. combined near-infrared (NIR) contrast agents with a handheld spectroscopic pen device to conduct SERS analysis on breast tumor-bearing mice. This approach allowed for the precise identification of tumor borders both preoperatively and intraoperatively. Dinish et al. used intratumoral injections of antibody-conjugated SERS nanotags to target three intrinsic cancer biomarkers—EGFR, CD44, and TGF-beta RII—in a breast cancer model. SERS signals were specifically detected in tumor-bearing animals, peaking six hours post-injection.

Karabeber et al. developed a handheld Raman scanner guided by SERS nanoparticles to identify tumor tissues in a genetically engineered RCAS/tv-a glioblastoma mouse model. This method demonstrated greater accuracy than conventional white light visualization. Harmsen et al. introduced a next-generation SERS nanoparticle system capable of precisely visualizing tumor margins, invasion, and locoregional spread in mouse models of pancreatic, breast, prostate, and sarcoma cancers.

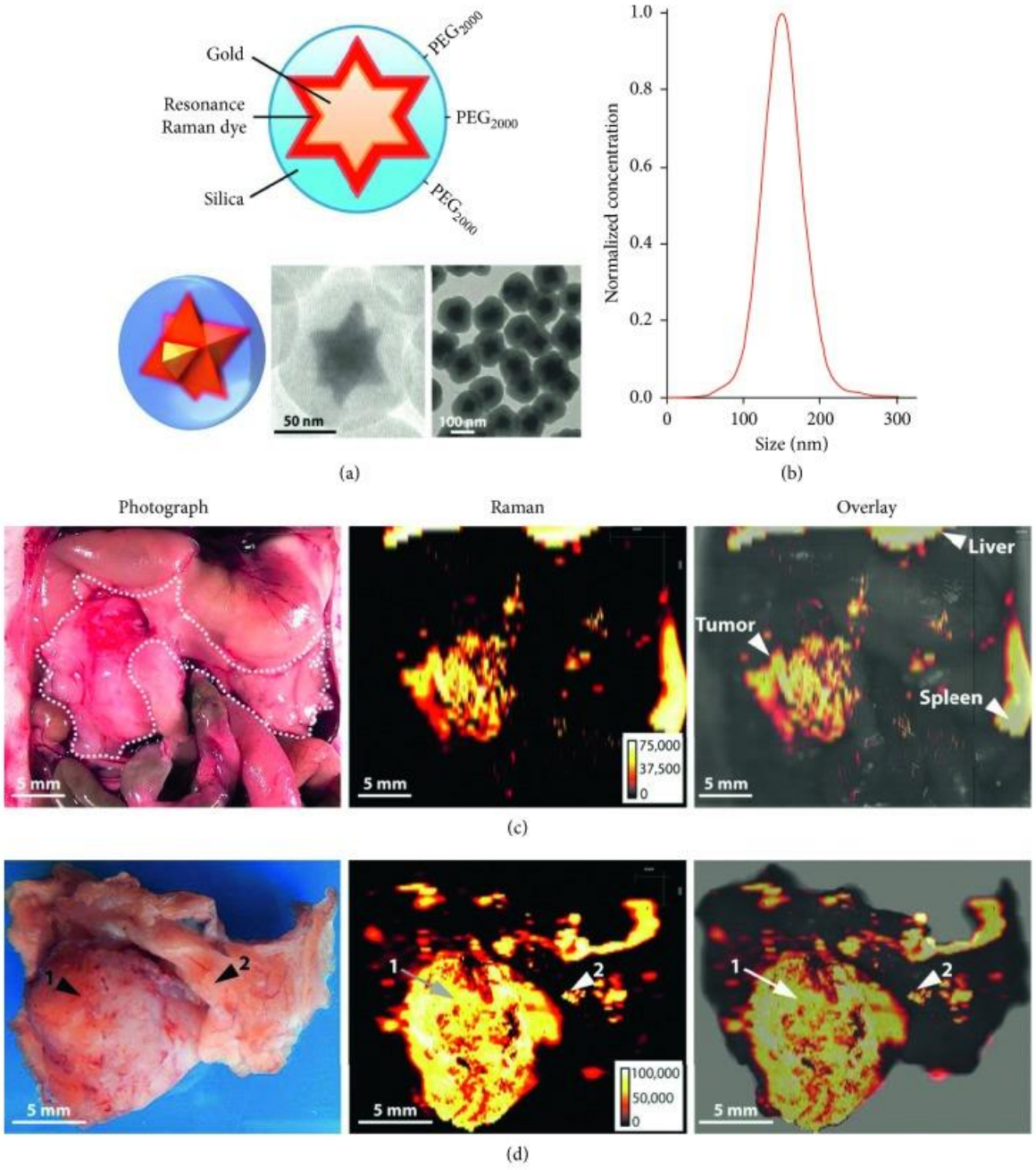

Figure 4. A new generation of SERS nanoparticles designed for precise visualization of tumor margins, invasion, and locoregional spread. (a) Nanoparticle structure; (b) nanoparticle size distribution; (c) in situ image of the exposed upper abdomen in a mouse with pancreatic cancer in the head of the pancreas (outlined with a white dotted line), alongside a Raman image showing SERRS-nanostar signals in the visible tumor and scattered foci in other normal-appearing areas of the pancreas; (d) photographic and high-resolution Raman images of the excised pancreas from (c).

4.2.2. Studies in Humans

Garai et al. recently developed a compact, noncontact optoelectromechanical Raman device that attaches to clinical endoscopes. This innovative device, used in conjunction with a

series of SERS nanoparticles, significantly enhanced the accuracy and speed of gastrointestinal cancer diagnosis.

5. Integration of Raman-Based Technologies with Other Optical Modalities for Cancer Diagnosis

5.1. Ex Vivo

The Popp group integrated Raman spectroscopy, coherent anti-Stokes Raman scattering (CARS), second harmonic generation (SHG), and two-photon-excited fluorescence (TPEF) imaging into a single platform. This multimodal approach produced distinct images of basal cell and squamous cell carcinoma. They further applied multimodal nonlinear imaging to ex vivo brain tissues, identifying cytological and architectural features critical for tumor grading.

5.2. In Vivo

Kircher et al. developed a unique triple-modality nanoparticle combining magnetic resonance imaging (MRI), photoacoustic imaging, and Raman imaging for selective visualization of tumor margins in glioblastoma-bearing mice. Jeong et al. created a dual-modal fluorescence-Raman endomicroscopic system that uses fluorescence and SERS nanoprobes to simultaneously detect two biomarkers—human epidermal growth factor receptor 2 (HER2) and epidermal growth factor receptor (EGFR)—in a breast cancer orthotopic model. Kim et al. demonstrated the application of this system for colorectal cancer diagnosis in an orthotopic xenograft model.

Lin et al. introduced a four-modality integrated endoscopy system combining white light imaging, autofluorescence imaging, diffuse reflectance spectroscopy, and Raman spectroscopy. This system was used for in vivo detection of nasopharyngeal cancer during endoscopic procedures.

6. Conclusions

Raman scattering-based techniques provide powerful tools for cancer diagnosis due to their ability to perform label-free, highly sensitive analysis of biomolecules in situ. Utilizing fiber-optic-based light delivery and collection, these techniques are predominantly applied to accessible tissue surfaces, such as the skin, gastrointestinal tract, or during surgical procedures. Their key advantage lies in their high sensitivity and specificity, enabling rapid and accurate differentiation between malignant, premalignant, and normal tissues. However, a persistent challenge remains: identifying highly specific molecular markers for various types of human cancers. Hyperspectral SRS microscopy, capable of quantitatively mapping diverse molecular species, presents a promising approach for discovering novel molecular markers for cancer diagnosis.

EURASIAN JOURNAL OF MEDICAL AND NATURAL SCIENCES
Innovative Academy Research Support Center
IF = 7.921
www.in-academy.uz

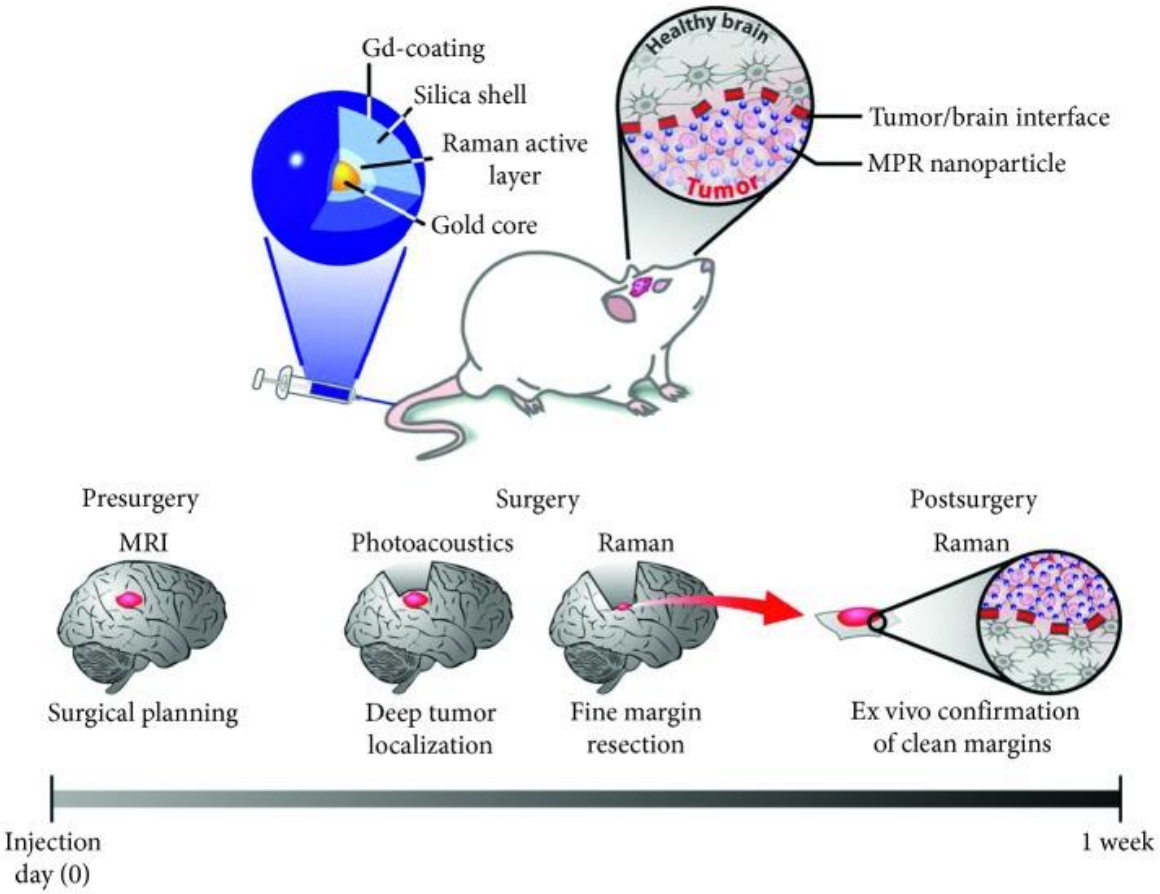

(a)

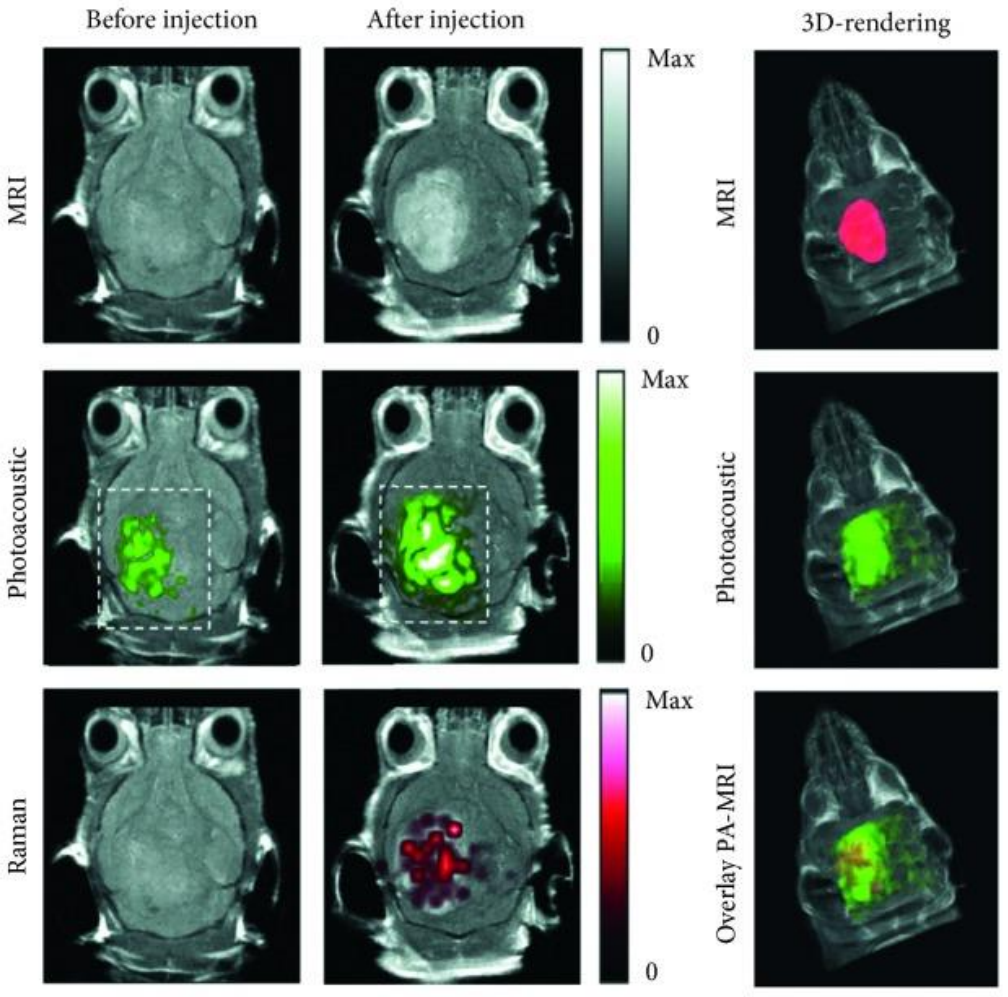

(b) (c)

Figure 5. A novel triple-modality nanoparticle combining magnetic resonance imaging (MRI), photoacoustic imaging, and Raman imaging (MPR) for precise multimodal visualization of tumor margins in glioblastoma-bearing mice. (a) Concept of the MPR nanoparticle; (b, c) three weeks after orthotopic inoculation, tumor-bearing mice (n = 4) received intravenous injections of MPR nanoparticles (16 nm, 170 μl). Brain images (with skin and skull intact) were acquired using photoacoustic, Raman, and MRI modalities before and at 2, 3, and 4 hours post-injection. (b) 2D axial MRI, photoacoustic, and Raman images post-injection demonstrated clear tumor visualization, with photoacoustic and Raman images coregistered with MRI, showing excellent colocalization among the three modalities. (c) 3D rendering of MR images with segmented tumor (red, top); overlay of 3D photoacoustic images (green) on MRI (middle); and a combined overlay of MRI, segmented tumor, and photoacoustic images (bottom), highlighting precise colocalization of the photoacoustic signal with the tumor.

References:

1. Santos I. P., Barroso E. M., Schut T. C. B., et al. Raman spectroscopy for cancer detection and cancer surgery guidance: translation to the clinics. Analyst. 2017;142(17):3025–3047. doi: 10.1039/c7an00957g. [DOI] [PubMed] [Google Scholar]
2. Downes A. Raman microscopy and associated techniques for label-free imaging of cancer tissue. Applied Spectroscopy Reviews. 2015;50(8):641–653. doi: 10.1080/05704928.2015.1052817. [DOI] [Google Scholar]
3. Pence I., Mahadevan-Jansen A. Clinical instrumentation and applications of Raman spectroscopy. Chemical Society Reviews. 2016;45(7):1958–1979. doi: 10.1039/c5cs00581g. [DOI] [PMC free article] [PubMed] [Google Scholar]
4. Jermyn M., Desroches J., Aubertin K., et al. A review of Raman spectroscopy advances with an emphasis on clinical translation challenges in oncology. Physics in Medicine and Biology. 2016;61(23):R370–R400. doi: 10.1088/0031-9155/61/23/r370. [DOI] [PubMed] [Google Scholar]
5. Austin L. A., Osseiran S., Evans C. L. Raman technologies in cancer diagnostics. Analyst. 2016;141(2):476–503. doi: 10.1039/c5an01786f. [DOI] [PubMed] [Google Scholar]
6. Cheng J. X., Xie X. S. Coherent Raman Scattering Microscopy. Boca Raton, FL, USA: CRC Press; 2012. [Google Scholar]
7. Yue S., Cheng J. X. Deciphering single cell metabolism by coherent Raman scattering microscopy. Current Opinion in Chemical Biology. 2016;33:46–57. doi: 10.1016/j.cbpa.2016.05.016. [DOI] [PMC free article] [PubMed] [Google Scholar]
8. Freudiger C. W., Min W., Saar B. G., et al. Label-free biomedical imaging with high sensitivity by stimulated Raman scattering microscopy. Science. 2008;322(5909):1857–1861. doi: 10.1126/science.1165758. [DOI] [PMC free article] [PubMed] [Google Scholar]
9. Nandakumar P., Kovalev A., Volkmer A. Vibrational imaging based on stimulated Raman scattering microscopy. New Journal of Physics. 2009;11(3):p. 033026. doi: 10.1088/1367-2630/11/3/033026. [DOI] [Google Scholar]
10. Ozeki Y., Dake F., Kajiyama S., Fukui K., Itoh K. Analysis and experimental assessment of the sensitivity of stimulated Raman scattering microscopy. Optics Express. 2009;17(5):3651–3658. doi: 10.1364/oe.17.003651. [DOI] [PubMed] [Google Scholar]

11. Slipchenko M., Oglesbee R. A., Zhang D., Wu W., Cheng J. X. Heterodyne detected nonlinear optical microscopy in a lock-in free manner. Journal of Biophotonics. 2012;5(10):801–807. doi: 10.1002/jbio.201200005. [DOI] [PubMed] [Google Scholar]
12. Darrigues E., Nima Z. A., Majeed W., et al. Raman spectroscopy using plasmonic and carbon-based nanoparticles for cancer detection, diagnosis, and treatment guidance. Part 1: diagnosis. Drug Metabolism Reviews. 2017;49(2):212–252. doi: 10.1080/03602532.2017.1302465. [DOI] [PubMed] [Google Scholar]
13. Kendall C., Day J., Hutchings J., et al. Evaluation of Raman probe for oesophageal cancer diagnostics. Analyst. 2010;135(12):3038–3041. doi: 10.1039/c0an00536c. [DOI] [PubMed] [Google Scholar]
14. Bhattacharjee T., Khan A., Maru G., Ingle A., Krishna C. M. A preliminary Raman spectroscopic study of urine: diagnosis of breast cancer in animal models. Analyst. 2015;140(2):456–466. doi: 10.1039/c4an01703j. [DOI] [PubMed] [Google Scholar]
15. Elumalai B., Prakasarao A., Ganesan B., Dornadula K., Ganesan S. Raman spectroscopic characterization of urine of normal and oral cancer subjects. Journal of Raman Spectroscopy. 2015;46(1):84–93. doi: 10.1002/jrs.4601. [DOI] [Google Scholar]
16. Sahu A., Sawant S., Mamgain H., Krishna C. M. Raman spectroscopy of serum: an exploratory study for detection of oral cancers. Analyst. 2013;138(14):4161–4174. doi: 10.1039/c3an00308f. [DOI] [PubMed] [Google Scholar]
17. Sahu A., Nandakumar N., Sawant S., Krishna C. M. Recurrence prediction in oral cancers: a serum Raman spectroscopy study. Analyst. 2015;140(7):2294–2301. doi: 10.1039/c4an01860e. [DOI] [PubMed] [Google Scholar]
18. Almond L. M., Hutchings J., Lloyd G., et al. Endoscopic Raman spectroscopy enables objective diagnosis of dysplasia in Barrett's esophagus. Gastrointestinal Endoscopy. 2014;79(1):37–45. doi: 10.1016/j.gie.2013.05.028. [DOI] [PubMed] [Google Scholar]
19. Hsu C. W., Huang C. C., et al. Differentiating gastrointestinal stromal tumors from gastric adenocarcinomas and normal mucosae using confocal Raman microspectroscopy. Journal of Biomedical Optics. 2016;21(7):p. 075006. doi: 10.1117/1.jbo.21.7.075006. [DOI] [PubMed] [Google Scholar]
20. Hsu C. W., Huang C. C., Sheu J. H., et al. Novel method for differentiating histological types of gastric adenocarcinoma by using confocal Raman microspectroscopy. PLos One. 2016;11(7) doi: 10.1371/journal.pone.0159829.e0159829 [DOI] [PMC free article] [PubMed] [Google Scholar]